Quantitative Decoding of Interactions in Tunable Nanomagnet Arrays Using First Order Reversal Curves

Dustin A. Gilbert,[1] Gergely T. Zimanyi,[1] Randy K. Dumas,[1] Michael Winklhofer,[2]

Alicia Gomez,[3] Nasim Eibagi,[1] J. L.Vicent,[3,4] and Kai Liu[1]

[1]*Dept. of Physics, University of California, Davis, California, 95616, USA*

[2]*Dept. of Earth & Environmental Sciences, Ludwig-Maximilians-Universität München, Germany*

[3]*Dept. Fisica Materiales, Universidad Complutense, 28040 Madrid, Spain*

[4]*IMDEA-Nanociencia, Cantoblanco 28049, Madrid, Spain*

Supplemental Material

Experiments-Demagnetizing arrays: The physics of interactions were probed with the FORC technique by measuring six arrays where the interactions were systematically tuned. Two of the measured FORC diagrams were highlighted in Figs. 1 and 2 in the main text. This Supplemental material presents the full set, to demonstrate the experimental trends. Figure S1 shows the experimentally determined family of FORCs, the corresponding measured FORC distribution and the simulated FORC distribution. Here the demagnetizing interactions are strongest for array A1 (left column) and weakest for A3 (right column).

The families of FORCs become increasingly sheared with increasing interactions (top row, A3→A2→A1). Shearing of the hysteresis loops has been previously observed and is caused by mean-field demagnetizing interactions. The experimental FORC distributions exhibit a ridge aligned with the local coercivity H_C axis, shifted in the $+H_B$ direction at the low-H_C end, the shift increasing with increasing interaction strength (center and bottom rows, right to left). The high-H_C end of the FORC ridge remains on the H_C axis (H_B=0), while the extent or length of the ridge increases with increasing interaction strength, stretching the ridge.

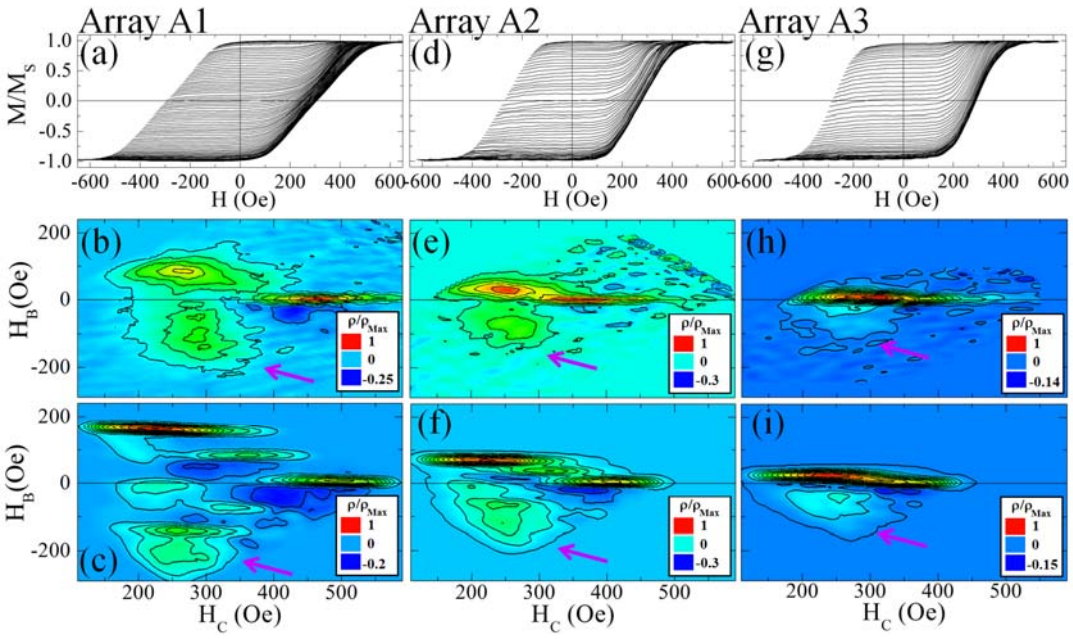

Fig. S1: *Experimentally determined family of FORCs (top row) and FORC distributions (middle row), and simulated FORC distributions (bottom row) for array A1 (panels a-c), A2 (panels d-f), and A3 (panels g-i). Vertical edge is identified by the purple arrow.*

In addition, an edge directed along the -H_B direction develops, highlighted by the arrow in Fig. S1, attached to the ridge at the low-H_C end. The edge becomes more extended with stronger interactions. A negative feature also develops underneath the high-H_C end. All these trends are consistent with the simulations and the predictions of the mean-field theory.

In addition, in Fig. S1 both the experiments and the simulations show that the ridge and the edge are not smooth but segmented. Segmenting is caused by the nearest neighbor interactions, as explained in the main text and in relation to Fig. S3 below.

Experiments-Magnetizing arrays: FORC diagrams for the magnetizing arrays B1/2/3 are shown in Fig. S2. The family of FORCs becomes *less* sheared (more square) with increasing interactions (top row, B3→B2→B1), in contrast to the demagnetizing case. The FORC distributions exhibit a ridge aligned with the H_C axis, shifted in the -H_B direction at the low-H_C end. The shift increases with increasing interaction strength (center and bottom rows, right to

left). The high-H_C end of the FORC ridge remains on the H_C axis (H_B=0), while the extent of the ridge along H_C decreases with increasing interaction strength – the ridge becomes compressed. Lastly, a negative edge develops below the ridge. Similarly to Fig. S1, all trends of the experimental results are reproduced in the simulated results.

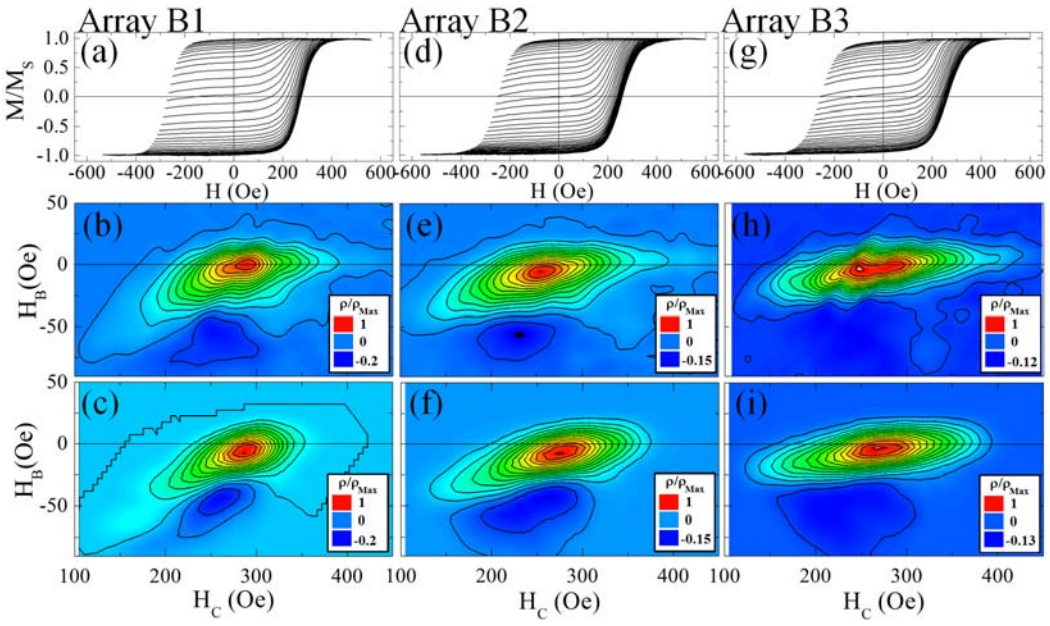

Fig. S2: *Experimentally determined family of FORCs (top row) and FORC distributions (middle row), as well as simulated FORC distributions (bottom row) for array B1(panels a-c), B2 (panels d-f), and B3 (panels g-i).*

The features and trends exhibited by the magnetizing arrays are explained next based on the mean field theory of the FORC diagrams, analogous to the demagnetizing interactions in the main text. Specifically, on each FORC curve, the highest coercivity down-flipped particle was the last to down-flip at H_{dn}=-H_K^i-$\alpha M(H_R)$, since it experienced a mean field $\alpha M(H_R)$.

The same highest coercivity particle on each FORC curve is the last to up-flip at H_{up}= H_K^i-αM_S, as the array reaches full saturation. As for the demagnetizing case, the corresponding last *dM/dH* jump on each FORC(H, H_R=-H_K^i-$\alpha M(H_R)$) is *unmatched* by the neighboring FORC(H,H_R>-H_K^i-$\alpha M(H_R)$) which differs only in that $P(H_K^i)$ was un-flipped along that FORC.

These unmatched *dM/dH* jumps generate the FORC-ridge aligned with the H_C axis.

In complete analogy to the demagnetizing case, the ridge is shifted off the H_C axis at the low-H_C end by $-\alpha M_S$, but because $\alpha>0$ for the magnetizing case, the shift is in the $-H_B$ direction. Further, the high-H_C end of the ridge, again staying on the H_C axis, gets "stretched" by $-\alpha M_S$, but since $\alpha>0$, this actually means a *compression*.

The appearance of the edge, attached to the ridge at the low-H_C end, can also be understood from arguments analogous to the ones explaining the vertical edge in the demagnetizing case. The first up-flip along each FORC, performed by the lowest coercivity particle H_K^{Min}, is biased by $\alpha M(H_R)$, up-flipping at $H_{up}=H_K^{Min}-\alpha M(H_R)$. For the least negative H_R reversal fields $M(H_R)$ is close to M_S and the mean field reduces the up-flip field H_{up} by the largest amount-αM_S. For increasingly negative H_R values the magnetization $M(H_R)$ is decreasing, therefore the mean field interactions *reduce H_{up} by a decreasing amount*, in effect shifting the up-flip field H_{up} to increasingly positive values, as shown in FIG. 3e, right panel in the main text.

This shift again makes the first *dM/dH* jumps of the FORCs *unmatched*, but this time by the neighboring FORC with a more negative H_R. Moreover, visibly for these magnetizing interactions the value of the *dM/dH* jump changes from positive to zero, making them unmatched. Thus the magnetizing interactions again create the edge but this time with a negative amplitude.

Nearest Neighbor Interactions – demagnetizing model: It is noticed that the measured FORC diagrams exhibit the ridge-and-edge structures, but for the demagnetizing arrays these features are segmented, not smooth. For some of the arrays, the segments are in fact separated from each other.

In an attempt to account for this segmentation of the ridge and edge, in our simulations we chose to augment the mean interaction field with terms explicitly representing the nearest neighbor dipolar interactions, since these are the largest energy terms treated only approximately within the mean field. This extension of the mean field theory can be viewed as including the first terms of a systematic cluster expansion.

As shown in Fig. S1 (c), (f), and (i), the inclusion of nearest neighbor terms in the simulations indeed segment the FORC ridge and edge, verifying our expectations. To understand the effect and phenomenology of the nearest neighbor terms, we now construct a theoretical analysis of the FORC diagram of nearest-neighbor-only models, and then integrate the nearest-neighbor-only model into mean field framework.

As shown in Fig. S3(b), the experimentally relevant two-dimensional demagnetizing arrays with nearest-neighbor-only interactions exhibit three well-defined primary peaks (P1-P3) and three secondary peaks (P4-P6) in the FORC distribution. These features can be directly identified with specific up- and down- switching events. As shown in Fig. 1(a) of the main text, since the coupling of any dipole is strongest to the two nearest neighbors along the minor axis, the interactions can be represented by defining the directions of these three dipoles.

With this convention, and denoting the nearest neighbor interaction field with $H_{n.n.}$, the down-flipping events are:

(D1) positive saturation → checkerboard (↑↑↑ → ↑↓↑: $H_{int}=2H_{n.n.}$),

(D2) checkerboard → negative saturation (↓↑↓ → ↓↓↓: $H_{int}= -2H_{n.n.}$), and

(D3) frustrated checkerboard → frustrated checkerboard (↓↑↑ →↓↓↑: $H_{int}=0$).

The up-flipping events are:

(U1) checkerboard → positive saturation (↑↓↑ → ↑↑↑: $H_{int}=2H_{n.n.}$),

(U2) negative saturation → checkerboard (↓↓↓→ ↓↑↓: H_{int}= -2$H_{n.n.}$), and

(U3) frustrated checkerboard → frustrated checkerboard (↓↓↑ →↓↑↑: H_{int}=0).

Using the switching conditions discussed in the text, we now describe how each peak in the FORC distribution is generated by a FORC curve, defined by a down-flip and an up-flip. In particular:

- the peak P1 at (H_C=H_K, H_B=+2$H_{n.n.}$) is generated by the FORC with the D1 and U1 flips;

- the peak P2 at (H_C=H_K, H_B=-2$H_{n.n.}$) is generated by the FORC with the D2 and U2 flips;

- the peak P3 at (H_C=H_K+2$H_{n.n.}$, H_B=0) is generated by the FORC with the D2 and U1 flips;

- the peak P4 at (H_C=H_K+$H_{n.n.}$, H_B=+$H_{n.n.}$) is generated by the FORC with the D3 and U1 flips;

- the peak P5 at (H_C=H_K+$H_{n.n.}$, H_B=-$H_{n.n.}$) is generated by the FORC with the D2 and U3 flips; and

- the peak P6 at (H_C=H_K, H_B=0) is generated by the FORC with the D3 and U3 flips.

Visibly, the amplitudes of peaks P1 and P2 are the strongest. The reason for this is that the state the dipoles flip in-to and out-of when generating the peaks P1/P2 is the lowest energy anti-ferromagnetic state, thus favored by a majority of reversal pathways.

The peak P3 has the next-strongest amplitude. The reason for this is analogous to the above arguments, with the difference that while peaks P1/P2 are formed by flips *from* the saturated states *into* the checkerboard pattern, P3 is generated by high H_K dipoles flipping *from* the checkerboard *into* the saturated states. In sum, these three peaks are well defined because in the demagnetizing systems there exists an energetically favorable intermediate state, the checkerboard state, through which most reversal pathways go through.

In comparison, peaks P4/5/6 have much smaller amplitudes. This is due to the fact that the starting, ending, or both configurations are frustrated, with energies higher than the checkerboard state, and therefore any particular flip sequence is carried out only by a small fraction of the dipoles.

Further, the reversal of a single particle also reduces the interactions on its neighbors, and subsequently they are less likely to reverse, thus nucleating a local checkerboard ordering. Fig. S3(c) illustrates that these locally formed checkerboards tend to organize themselves into larger checkerboard patterns, highlighted by the green boxes. Fig. S3(f) illustrates, that, in contrast, the mean field theory does not capture these local checkerboard-ordering tendencies, and correspondingly, the mean field FORC distribution does not show the formation of localized peaks that could segment the smooth ridge-and-edge structure.

Therefore, to account for the experimentally observed segmenting of the ridge-and-edge structure, the mean field theory and the nearest-neighbor-only frameworks have to be combined. Fig. S3(h)-(i) show the FORC distribution and dipole configuration obtained by simulating the combined model. Both the formation of the ridge-and-edge structure and the 3+3 peaks structure are clearly recognizable in the FORC distribution. To sum-up the demagnetizing considerations, we conclude that both the theoretical analysis and simulations demonstrate that mean field plus nearest neighbor model fully explains all the features in the experimental FORC distributions.

Nearest Neighbor Interactions – magnetizing model: In the experimental systems with magnetizing interactions the FORC distributions was not strongly segmented like it was in the demagnetizing case. We attribute this absence of segmenting to the lack of a lower-energy intermediate state, as the checkerboard state was for the demagnetizing systems. As we show now, in the nearest-neighbor-only model the interactions guide the system from one saturated

state directly to the other without getting trapped in any intermediate state. Accordingly, the FORC distribution of these models is a single localized structure, as shown in Fig. S3(k).

In detail, the nearest neighbor magnetizing interactions cause an avalanche-like reversal of chains of dipoles. The effects of the nearest neighbor interactions in these magnetizing systems can be interpreted as follows: the interactions stabilize the parallel ordering between neighbors, aligned along the dipole axis. Therefore, when a dipole flips this *reduces* the stability of the remaining un-flipped dipoles. While the effect is small for the mean-field model, as $\Delta H_{int}=2\alpha M_S/N$, (where N is the total number of dipoles in the system), for nearest neighbor interactions the change in the interactions field is $\Delta H_{int}=2H_{n.n.}$, reducing the total interaction field to zero. This enables the external field to flip the neighboring dipole as well. Consequently, the flip of each dipole greatly de-stabilizes its neighbors and induces them to flip as well. As the neighbors flip, the destabilized front propagates to the next-nearest-neighbors, inducing an avalanche propagating down the chain of neighbors until a local high-coercivity particle ($H_K>2H_{n.n.}+H$) stops the avalanche. The dipoles participating in a single avalanche share the same down-flip and up-flip fields, and therefore contribute to the FORC distribution at a single (H_C,H_B) location, which we call the avalanche peak. This single avalanche peak may broaden somewhat for wide coercivity distributions, as the flip field of avalanches is impacted by dipoles with extreme coercivity values.

Fig. S3(n) shows that when the mean field and the nearest-neighbor-only models are combined, since the location of the single avalanche peak overlaps with the mean field ridge, the resulting FORC does not exhibit any segmenting. Rather, it shows a ridge with a well-formed maximum at the location of the avalanche peak.

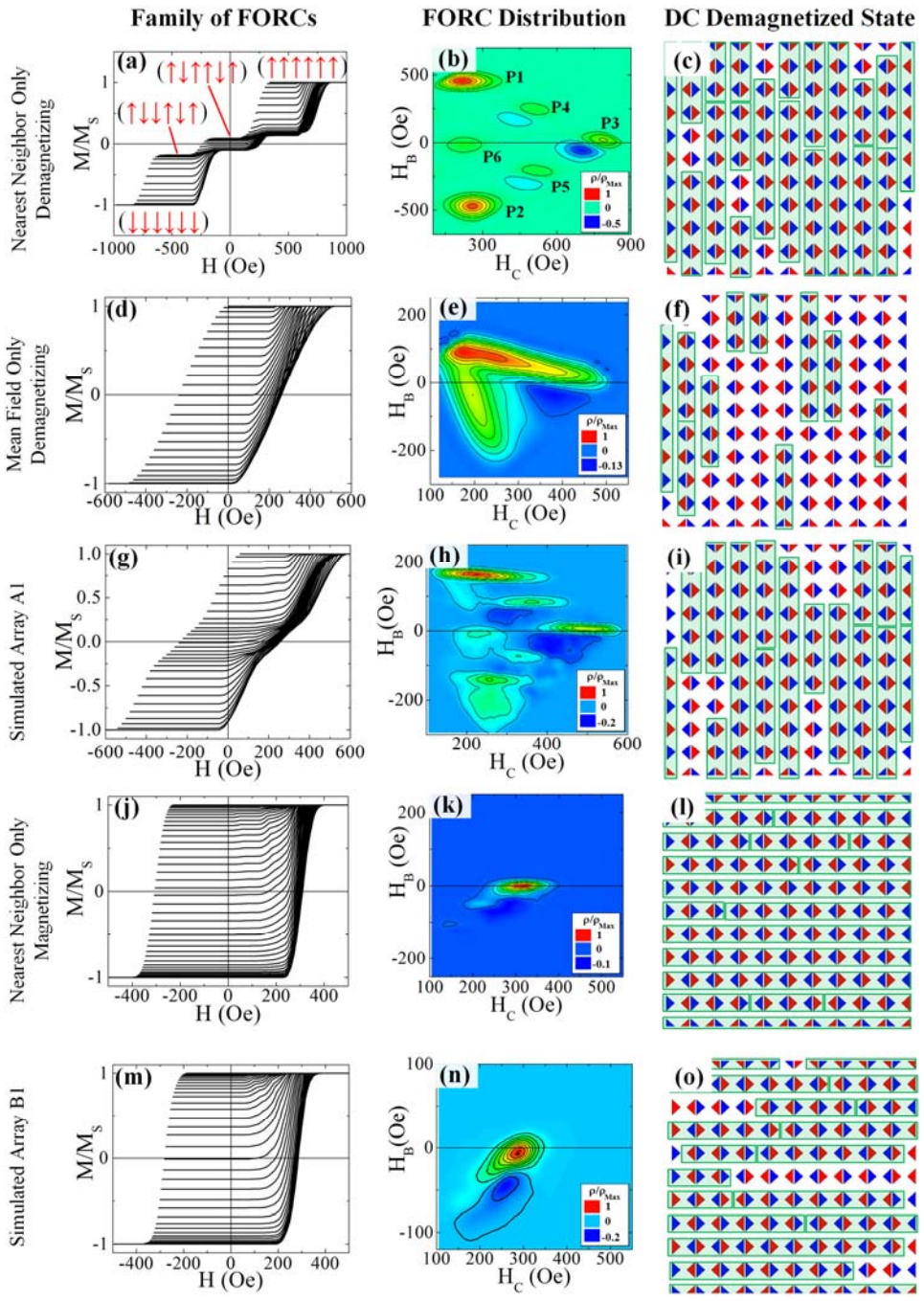

Fig. S3: *From left to right columns, simulated family of FORCs, FORC distributions and DC-demagnetized remnant states are shown for systems with (a-c) nearest neighbor (n.n.) demagnetizing; (d-f) mean-field (m.f.) demagnetizing; (g-i) combined (m.f.+n.n.) demagnetizing; (j-l) n.n. magnetizing; (m-o) combined (m.f.+n.n.) magnetizing interactions. In the right column, red/blue arrows represent dipole orientations and green boxes highlight local ordering.*